Available online at www.sciencedirect.com

jmr&t Journal of Materials Research and Technology

www.jmrt.com.br

Original Article

# Martensite reversion and texture formation in 17Mn-0.06C TRIP/TWIP steel after hot cold rolling and annealing

*Diana Pérez Escobar*, Sara Silva Ferreira de Dafé, Dagoberto Brandão Santos*

*Department of Metallurgical and Materials Engineering, Universidade Federal de Minas Gerais (UFMG), Belo Horizonte, MG, Brazil*

ARTICLE INFO

*Article history:*
Received 12 July 2014
Accepted 8 October 2014
Available online 4 November 2014

*Keywords:*
Texture
Electron backscattering diffraction (EBSD)
Cold rolling
Recrystallization
TRIP/TWIP steel

ABSTRACT

High Mn steels with Si and Al present great plasticity when deformed due to the TRIP/TWIP effect. This work evaluated the microstructural evolution and texture formation of a 17Mn-0.06C steel after hot rolling, cold rolling to 45% of thickness reduction and annealing at 700 °C for different times. The microstructural analysis was performed by means of dilatometry, X-ray diffraction (XRD), optical (OM) and scanning electron microscopy (SEM), electron backscattering diffraction EBSD and transmission electron microscopy (TEM). It was found that during the cooling process, after the steel is annealed, the athermal $\varepsilon$ and $\alpha'$ martensites are formed. Tensile test results showed that the steel exhibits yield and tensile strength around 650 and 950 MPa with a total elongation around 45%. The austenite texture contains brass, copper and Goss components while the $\alpha'$ and $\varepsilon$ martensites textures contain rotated cube and prismatic and pyramidal fibers, respectively.



## 1. Introduction

Steels containing Mn, Si, and Al in high concentrations, exhibit high mechanical strength and plasticity when deformed, due to the mechanical twinning (TWIP steels) or to a martensitic transformation (TRIP steels) [1–3].

An important parameter determining the type of deformation mechanism in these steels is their stacking fault energy (SFE). According to Dumay et al. [4], for SFE values greater than 18 mJ/m$^2$, the TWIP effect tends to occur, while for lower values, the TRIP effect is predominant, with an $\alpha'$ martensite phase being formed for SFE smaller than 12 mJ/m$^2$. The SFE also depends on the chemical composition and test temperature of the steel. In alloys with a Mn content (wt%) less than 15%, the TRIP effect dominates, while for a Mn content higher than 25% the TWIP effect is dominant. On the other hand, in alloys with a Mn content between 15% and 25%, the TRIP and TWIP effects can coexist [5].

Mechanical properties of steels subjected to rolling and annealing are determined by the nature and intensity of the transformation texture, once the plastic anisotropy of a material is greatly dependent on the texture [6]. Thus, understanding the deformation and transformation texture

* *Corresponding author.*
E-mail: diana.perezescobar@gmail.com (D. Pérez Escobar).
http://dx.doi.org/10.1016/j.jmrt.2014.10.004

mechanisms in these alloys when subjected to external loads is extremely important because it determines the mechanical properties that make them suited for industrial applications, such as their mechanical strength, ductility, formability and crash absorption energy [7–9].

The industrial production of TRIP and TWIP steels always involves thermomechanical processes including hot deformation, cold rolling at room temperature, and annealing [1,8]. In all these stages, the steel undergoes thermal cycles involving heating and cooling [10].

Lu et al. [11,12] studied the evolution of microstructure and texture during cold rolling and subsequent annealing in a steel with 22Mn and 0.376C. During rolling, the deformation mechanisms were found to be the dislocations slip, mechanical twinning, the $\varepsilon$ martensite formation induced by deformation and generation of shear bands. At larger deformations, the brass type texture with a scattering for Goss texture was dominant for the austenite. A decrease in the Cu and S components was attributed to the preferential transformation to $\varepsilon$ martensite in Cu and S oriented grains. On the subsequent annealing, the $\varepsilon$ martensite transformed reversely to austenite by a diffusionless mechanism [11,12].

TWIP steel with low C and reduced Mn content has rarely been studied [13,14]. With low SFE, these steels are very interesting because they are prone to transform to martensite resulting in a greatly enhanced working hardening rate [4].

The present work investigated the microstructure evolution of a 17Mn-0.06 C steel (Table 1) after being subjected to hot (56% reduction at 1100 °C) and cold rolled (45% reduction) and subsequently annealed at 700 °C for different times. The effects of the microstructure on the steel in its mechanical behavior were also evaluated. The treatments were meant to produce an ultrafine-grained microstructure that exhibited the TRIP and TWIP effects. Even though the chemical composition of the steel used (low Mn and C content) as well as the processing has not been studied deeply in literature, the results found in this work are extremely important for the application of this steel in the automotive industry.

Until now the works have concentrated on high Mn-C steels with TWIP effect [11,12,15–21]. Only two references were found in the literature that are dealing with similar chemical composition [13,14], but these works do not present results from texture of the three phases involved in the entire transformation.

## 2. Methods

The chemical composition of the experimental steel used in this study is presented in Table 1. The steel was melted as a standard keel block, in open air using an induction furnace (Power Trak 250-10 R Inductotherm®). After casting, the material was austenitized at 1100 °C for 2 h and subsequently water-cooled in order to homogenize the microstructure and chemical composition. After homogenization, the samples were hot rolled at 1070 °C with four passes with the same reduction to a total thickness reduction of 50%. The final thickness was 12 mm. The material was then cold rolled in 7 passes to a total thickness reduction of 45%. The final thickness of the samples was 7 mm.

**Table 1 – Chemical composition of the steel (wt%).**

| Element | Mn | Al | Si | Ni | C |
|---|---|---|---|---|---|
| Weight percent | 17 | 3 | 2 | 1 | 0.06 |

The samples were then annealed at 700 °C for 60, 700, 1800 s and 7200 °C and cooled at room temperature to study the recrystallization.

Optical microscopy studies of the samples after annealing were performed. The samples were first etched with nital (10%) and then with Klemm's I etchant [22,23]. For the Scanning electron microscopy (SEM) measurements, the samples were etched with Villela etchant.

The X-ray diffraction (XRD) was performed at room temperature in a Philips PW 1710 diffractometer with Cu K$\alpha$ radiation. For the quantification of the austenite and the $\varepsilon$ and $\alpha$ martensites, the direct comparison method was used [15], which involves the integration of the most intense peaks of each phase characterized by the (1 1 1), (2 0 0), (2 2 0), and (3 1 1) planes of austenite, the (1 1 0), (2 0 0), (2 1 1), and (2 2 0) planes of ferrite, and the (1 0 0), (0 0 2), (1 0 1), and (1 0 2) planes of $\varepsilon$ martensite. The integration of the intensities was done with support of a graphic software (Origin™), following the methodology described by Dafé et al. [22].

Electron backscatter diffraction (EBSD) measurements were performed in order to quantify the microstructure and obtain the texture of the samples. For this analysis, the samples were additionally polished with colloidal silica with 0.05 μm particles. The EBSD/TSL-OIM system was installed on an FEI-Inspect S50W filament SEM.

Transmission electron microscopy (TEM) was also performed. Slices were cut and polished until 0.15 mm in the section normal direction (ND) – transversal direction (TD). Discs with a diameter of 3.0 mm were taken from these slices using a precision disk punch equipment and were ground until 70 μm thickness in a 1200 mesh grind paper, subsequently polished with diamond past of 1 μm and properly cleaned. To reduce the final thickness for producing the hole in the center for the TEM, a Struers 5 tenupol was used, with a flow rate of 20 V. The solution used contained 95% of methanol and 5% of perchloric acid and was kept under −30 °C. Gatan software was used for acquisition and post-processing of acquired images.

Tensile tests at room temperature with a strain rate of $10^{-3}$ $s^{-1}$ were also performed in order to verify the mechanical behavior of the steel.

## 3. Results

Fig. 1 shows the dilatometric curve obtained by heating the sample continuously, after cold rolling reduction of 45%, as well as the derivative of the curve. The test was performed at temperatures ranging from room temperature to 1000 °C using a heating rate of 1 °C/s.

The diffraction patterns of the samples cold rolled and annealed at 700 °C for 60, 1800 and 7200 s obtained by X-ray diffraction, are displayed in Fig. 2a, and Fig. 2b presents the volume fraction of each phase as function of annealing time.

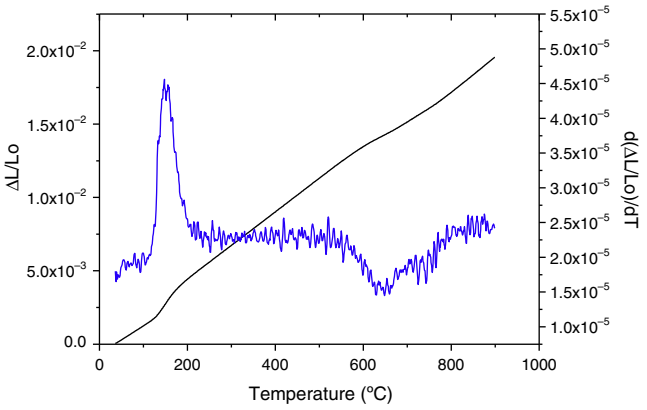


**Fig. 1 – Dilatometric curve and numerical derivative as function of the relative dilatation of the sample to cold rolling to 45% thickness reduction.**

The results of the XRD analyses reveal the presence of austenite as well as ε and α′ martensite phases (Fig. 2a). The volume fraction of α′ martensite phase is around 80% after cold rolling (Fig. 2b). On the other hand, in the case of the sample subjected to annealing at 700 °C for 1800 and 7200 s the relative amount of the austenite phase increased; this was accompanied by a decrease in the volume fraction of the ε martensite and the almost complete disappearance of the α′ martensite phase.

Fig. 3a and b shows the optical micrographs of the samples annealed at 700 °C after cold rolling with 45% of thickness reduction. Fig. 3c and d shows SEM micrographs of the samples annealed at 700 °C after same reduction and annealed for 60 and 1800 s. It is possible to see the deep etched α′ martensite phase and its amount decreases with increasing the annealing time, until the microstructure reaches a condition of well define polygonal austenite grains containing annealing twins, besides ε and α′ martensites, Fig. 3c and d. The ε martensite appears like plate forms and α′ martensite has the appearance of needles with very sharp edges. These characteristics are pointed out by arrows in Fig. 3d.

Fig. 4 presents the images obtained by TEM where it is possible to confirm that the sample is fully recrystallize after 1000 s due to the presence of annealing twins inside the austenite grains (Fig. 4a) and it is also possible to confirm the presence of ε martensite (Fig. 4b).

The IPF (inverse pole figure) and the image quality, IQ, from hot rolling condition, and then cold rolling, following by annealed samples at 700 °C for 60, 700, 1800, 3600 and 7200 s obtained by the OIM analysis software are displayed in Fig. 5. It can be seen from Fig. 5 that grain color for the hot, cold rolled and the annealed samples differ between themselves due to the fact that there is a pronounced changed in the orientation of the grains. It is possible to observe the α′ and ε martensite presence on the hot rolled microstructure as well as the evolution of the microstructure during annealing after the cold rolling. The different annealing times at 700 °C correspond to different volume fraction of martensite reversion, recrystallization and grain sizes.

Fig. 6 presents the textures resulting from hot rolling condition, cold rolling, following by annealed samples at 700 °C for 60, 700, 1800 and 7200 s. The texture is described by Pole Figure and Orientation Distribution Function (ODF) section $\varphi_2 = 45°$ and 65° for austenite, $\varphi_2 = 45°$ for α′ martensite (Fig. 6a) and $\varphi_2 = 30°$ for hcp phase, ε martensite (Fig. 6b). The analysis of the texture evolution during the recrystallization process gives more insight about the nucleation and grain growth mechanism. The texture for the ε martensite cold rolled is not presented because the amount of this phase in the sample was less than 10% and the authors judged that the result would not be reliable.

Finally, Fig. 7 presents the results of the tensile test performed for the sample cold rolled to 45%, for the same sample after annealing at 700 °C for 300 s and the true stress-strain and work hardening curve.

## 4. Discussion

The dilatometric result (Fig. 1) shows that a phase transformation occurred over the temperature range of 100–250 °C; this transformation was the reversion from ε martensite to austenite. For temperatures ranging from 500 to 700 °C, α′ martensite reverse transformation in austenite phase was observed. In

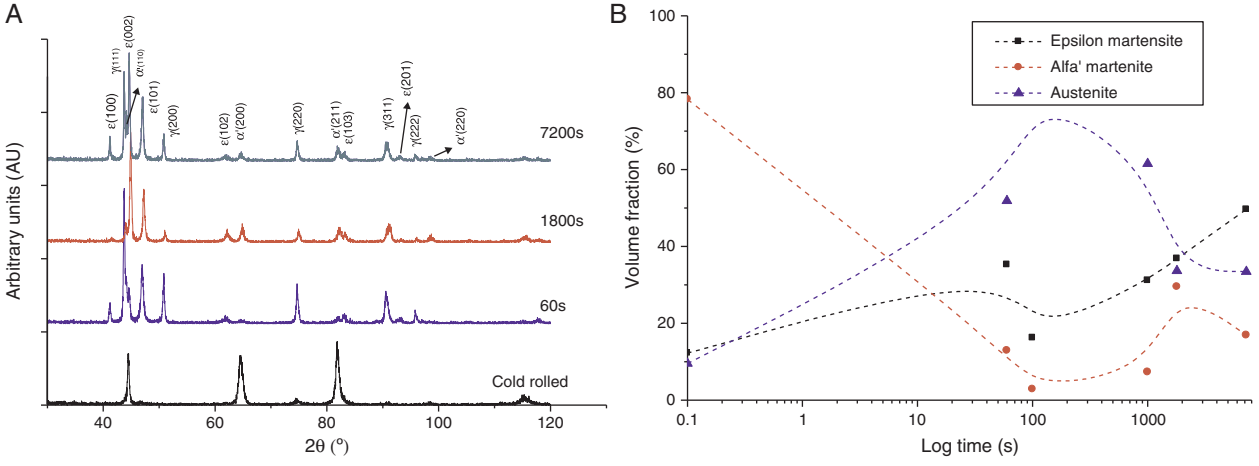


**Fig. 2 – (a) Diffraction patterns of the samples cold rolled and annealed at 700 °C for 60, 1800 and 7200 s. (b) Phase volume fraction of the samples cold rolled and annealed at 700 °C for different times.**

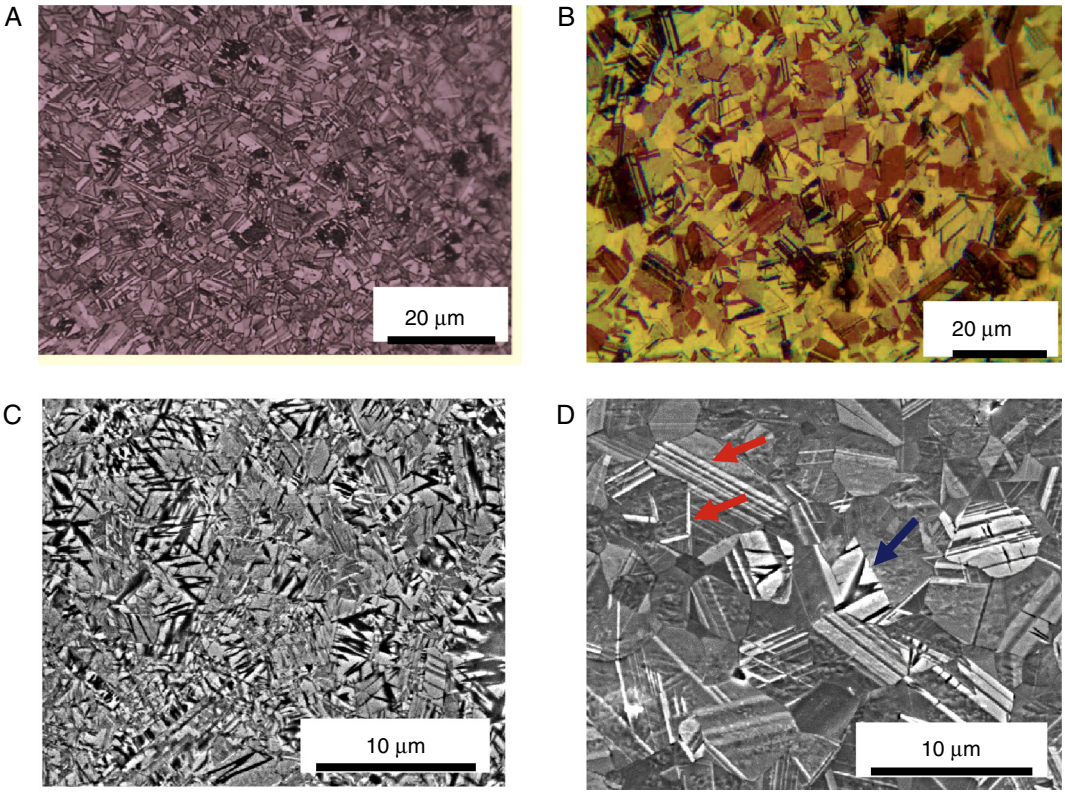


**Fig. 3 – Optical micrographs of the samples annealed at 700 °C after cold rolling with 45% of thickness reduction (a) 1800 s and (b) 7200 s. SEM micrographs of the samples annealed for (c) 60 s and (d) 1800 s. Etched with nital 10% plus Klemm I. Red arrow indicates $\varepsilon$ martensite and blue one indicate the $\alpha'$ martensite.**

order to be able to predict the deformation mechanisms of the various heat treated samples, their SFE values were estimated using the model proposed by Dumay et al. [4]. The value obtained was 14.5 mJ m$^{-2}$ [22,23], which indicates the occurrence of martensitic transformation as a plastic deformation mechanism, as well as mechanical twinning and dislocations slip. Dilatometric results demonstrate that the $\varepsilon$ martensite phase occurs in steel samples subjected to deformation, that is strain induced mode and having a low SFE. On the other hand, $\alpha'$ martensite phase is more likely to form initially from $\varepsilon$ martensite, which formed from austenite, $\gamma(\text{CFC}) \rightarrow \varepsilon(\text{HCP}) \rightarrow \alpha'$ (BCC). These observations were in agreement with the results reported in the literature [8–16]. These results were also in agreement with the XRD results that showed that a reduction

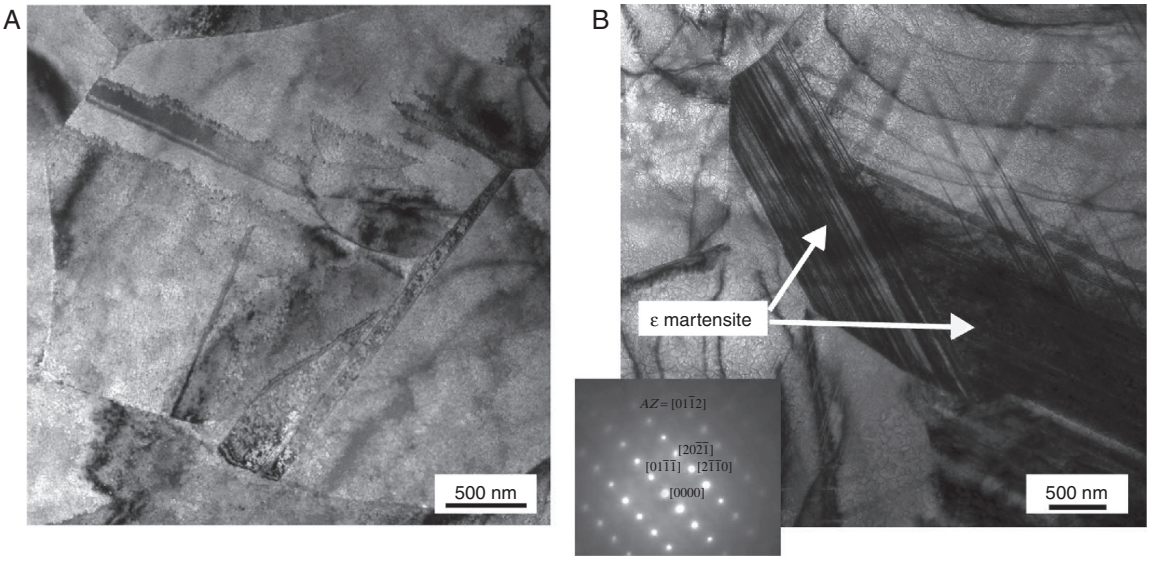


**Fig. 4 – Transmission electron microscopy (TEM) image of the $\varepsilon$ martensite with its respectively diffraction pattern (SADP).**

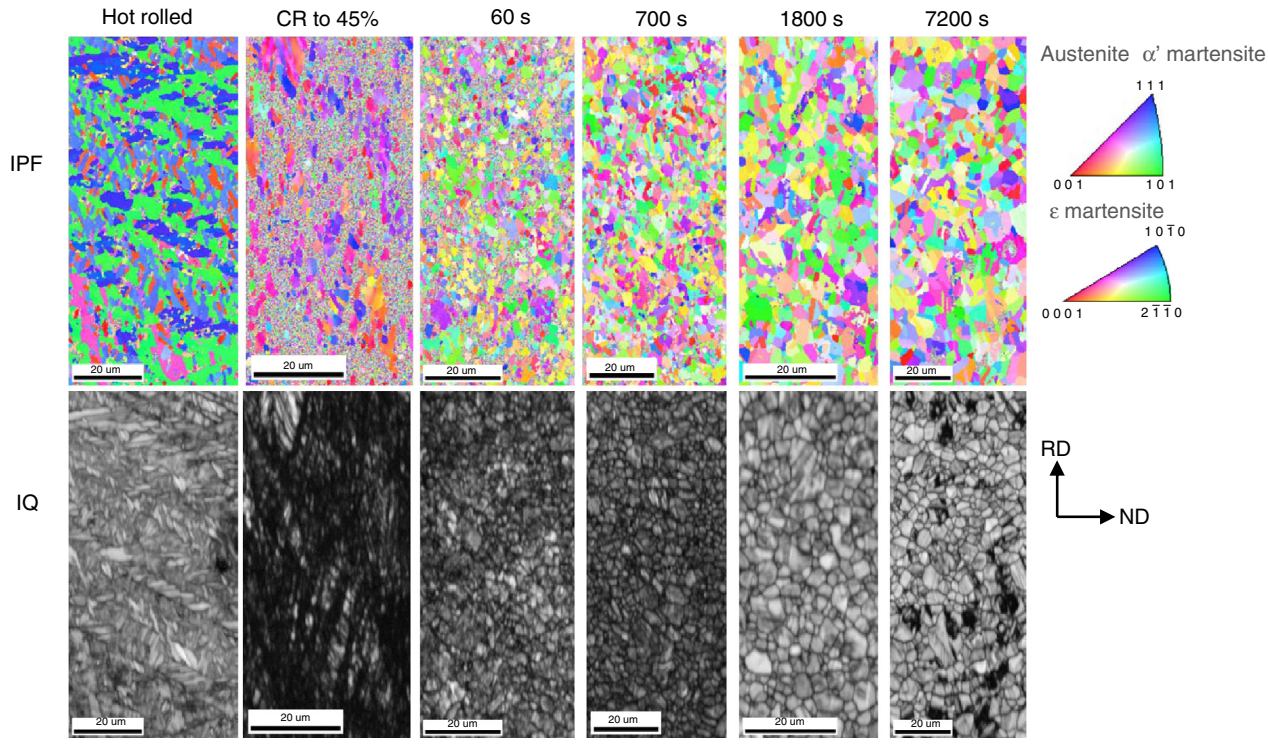


**Fig. 5 – IPF (inverse pole figure) and IQ (image quality) from hot rolling condition, and then cold rolling (CR), followed by annealed samples at 700 °C for 60, 700, 1800, 3600 and 7200 s.**

of 45% by cold rolling and subsequently annealing them at 700 °C resulted in a greater degree of martensite reversion, which starts around 200 °C according to Fig. 1, following by recrystallization of austenite at 700 °C. In cooling step from 700 °C, a great amount of ε martensite (50% volume fraction) is formed by athermal mode from the recrystallized austenite (Fig. 2b). TEM images (Fig. 4) together with the diffraction pattern indexation, corroborate the presence of the ε martensite in the sample. It is possible to observe that they form from shear bands.

Concerning the EBSD results, it is possible to observe that the hot-rolled texture of the austenite presents just a strong Goss component which is usual for austenite intensely deformed [24]. The α′ martensite has two components (1 1 1)[1 $\bar{1}$ 0] and (1 1 1)[0 1 $\bar{1}$] that belong to γ fiber. After the sample was cold-rolled, the texture of austenite changed abruptly to brass and S component (Fig. 6a). At this stage of cold rolling, the total thickness reduction was not sufficient to transform all austenite in α′ martensite. In this way the α′ martensite moved from α fiber to rotate cube (Fig. 6a) and a weak part on γ fiber still remained.

When α′ martensite reverts to austenite during annealing, two kinds of transformation texture can be expected. The austenite formed can recrystallize at the same time while the reversion process proceeds. If this simultaneous process occurs, the recrystallization texture is formed, whose intensity depends on the amount of strain accumulated before recrystallization. In this case, austenite shows Cube {1 0 0} <0 0 1> texture, which comes from Rotated Cube {0 0 1} <1 1 0>, Goss {1 1 0} <0 0 1> and Rotated Goss {0 1 1} <0 1 1> in α′ martensite. On the other hand, if there is no austenite recrystallization, this phase develops a relatively sharp texture containing Brass {1 1 0} <1 1 2>, Copper {1 1 2} <1 1 1> and S {1 2 3} <6 3 4>, besides Goss {1 1 0}<0 0 1> component. Texture results, shown in Fig. 6, proved that the α′ martensite reversion to austenite during annealing occurred without recrystallization. The main components in α′ martensite which give rise to texture in austenite, without recrystallization, are {3 3 2} <1 1 3> and {1 1 3} <1 1 0>, which promote in austenite Brass {1 1 0}<1 1 2> and Copper {1 1 2}<1 1 1> respectively. Grains with orientations belonging to α Fiber (<1 1 0> parallel to rolling direction) also give rise to the Copper in austenite. The transformation component S {1 2 3}<6 3 4> also tends to have their formation from α′ martensite orientations cited above, close to {1 1 2}<1 3 1> and also close to α Fiber components. The Goss {1 1 0}<0 0 1> component in the austenite originates in α′ martensite being part of them form Rotated Cu {1 1 2}<0 1 1>, or in components of γ Fiber ({1 1 1} parallel to rolling plane), such as {1 1 1}<1 1 0>, and some parts also in α Fiber [24–28]. The typical recrystallization component for the CFC metals is cube and its intensity increases with previous cold reduction and with annealing temperature [26]. In most CFC metals, the recrystallization is characterized by a mixture of cube with other components common to the deformation texture and as it has been found in literature [16,18–20], in some cases the cube component is not present in the alloy, which was the case of the present work. For longer annealing times the intensity of the copper component increased, which has been commonly found on the recrystallized samples [3,11–20,24].

The reverse transformation from ε and α′ martensite to austenite on annealing can happen in two ways: by a diffusional or displacive mechanism [24]. After longer annealing

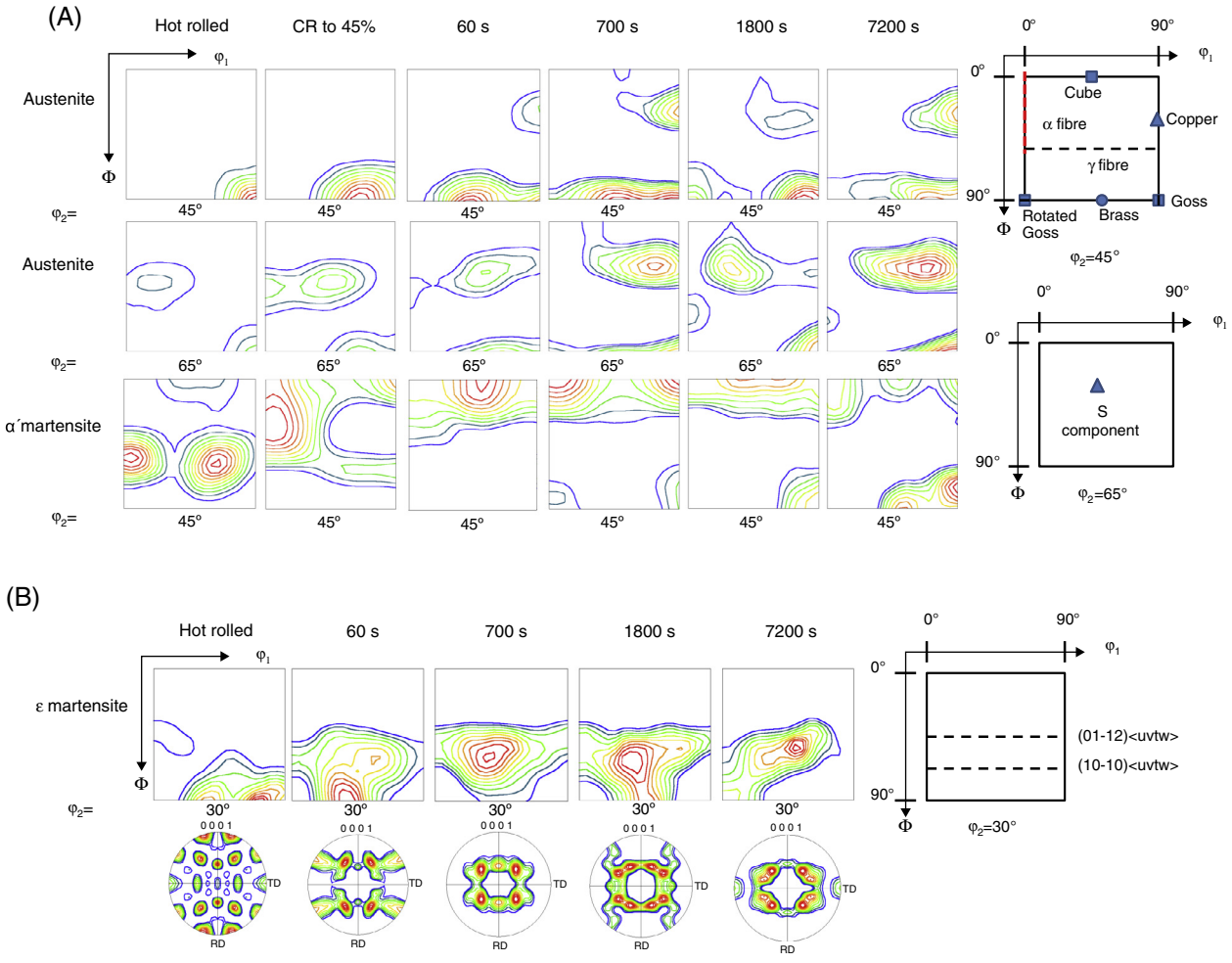


**Fig. 6 – Texture development as a function of annealing time. EBSD Images of IPF (inverse pole figure). Hot rolled, cold rolled, and annealed samples: 60, 700, 1800 and 7200 s for (a) austenite and α′ martensite and (b) ε martensite.**

times, there is a decline in the intensity of Cu and S orientations for the austenite, 1800 and 7200 s, which is accounted for by the transformation of ε martensite into grains with the same orientations. The brass and Goss components of the matrix are not favorable for the transformation so they remain and constitute the texture of the austenite, which is further stabilized by shear banding [11,16]. This effect, combined with the fast recrystallization kinetics and the orientated growth mechanism, leads to a very fine homogenous microstructure with a defined texture although this has been differently reported by Bouaziz et al. [5].

The textures of hexagonal metals and alloys can be categorized into three groups according to their *c*/*a* ratios, namely materials with *c*/*a* ratios greater than, approximately equal to, and less than the ideal value of 1.633. Metals and alloys with *c*/*a* ratios approximately equal to the ideal *c*/*a* ratio of 1.633, such as Mg, tend to form basal fiber textures during rolling. Metals and alloys with *c*/*a* ratios above the ideal, such as Zn (1.856) and Cd (1.885), tend to exhibit textures with basal poles tilted ±15–25° away from the normal direction toward the rolling direction and metals and alloys, possessing *c*/*a* ratio less than 1.633 such as Zr (1.589) and Ti (1.587), tend to form textures with basal poles tilted ±20–40° away from the normal direction toward the transverse direction [29]. ε martensite has a *c*/*a* ratio lower than 1.633 [30,31], the same as Zr and Ti, and the pole figures found in this work corresponded with the ones found in literature for metals with *c*/*a* < 1.633 [29]. The ODF of the ε martensite texture has not been intense discussed in the literature, even though studies on the pole figures are found [30,32]. The ODF for ε martensite are presented in Fig. 6b and shown a texture between a prismatic $(1\,0\,\bar{1}\,0)$ <*uvtw*> and pyramidal $(0\,1\,\bar{1}\,2)$ <*uvtw*> fiber for the hot rolled sample that continues to reinforce after annealing. This type of texture has been found for Zr alloys [33,34]. The presence of the ε martensite was confirmed by TEM presented in Fig. 4 together with the SAD (selected area diffraction) which has also been found in literature [5,11,32] for different alloys.

The recrystallization texture of deformed metals can be described in two ways [5,35,36]: (i) the oriented nucleation mechanism, where the recrystallized texture depends on the new nuclei orientation, and (ii) the selective growth mechanism, where the final recrystallized texture is not determined by the first nuclei orientations. The evolution of the texture during the recrystallization process in this work, clearly points in the direction of the selective growth mechanism. Moreover, contrary to observed by Bracke et al. [18–20], a discrete grain

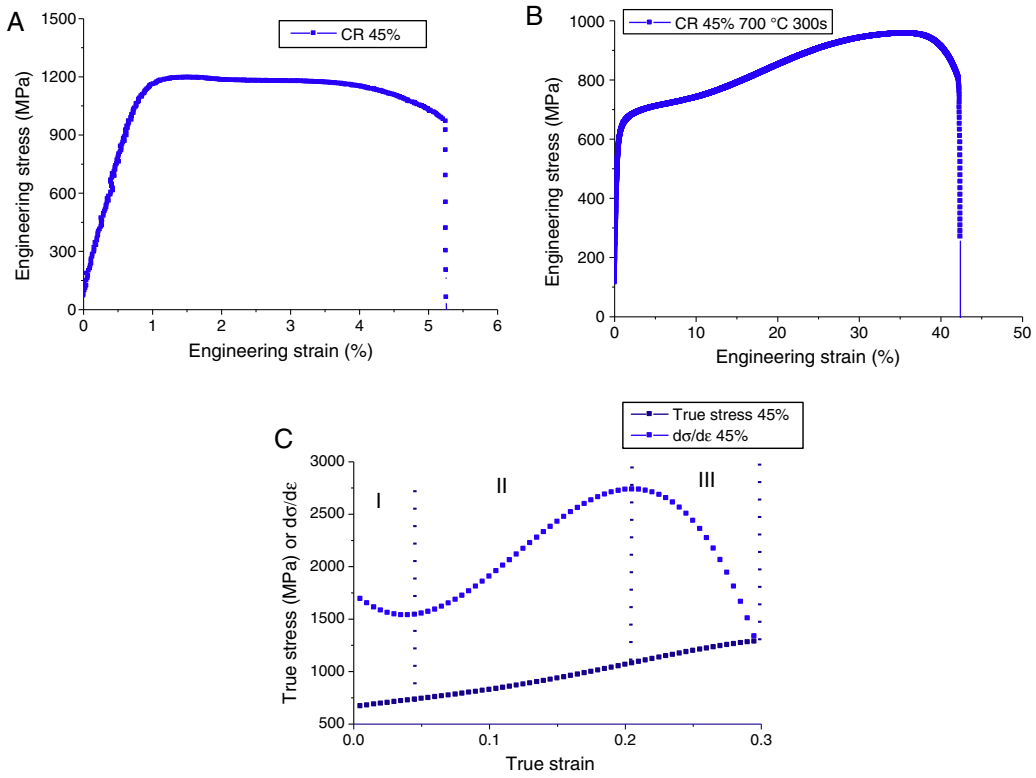


**Fig. 7 – Engineering stress–strain curve for the sample (a) cold rolled to 45% and (b) annealed at 700 °C for 300 s (c) and true stress–strain curve with work hardening results for the sample annealed at 700 °C for 300 s.**

growth is observed during recrystallization in the present steel (Fig. 5), a phenomenon that is more often observed in less textured material. In fact, the intensity of the cold deformed texture components decreases on the annealed samples, due to the multiplicity of the parent constituents. This refinement of the final microstructure through martensite reversion into austenite usually induces a good formability without strength loss [37,38].

Finally, the engineering stress-strain curve results (Fig. 7a and b) revealed a yield and tensile strength values of 1200 MPa for the cold rolled sample and 650 MPa and 950 MPa, respectively, for the annealed sample with a total elongation around 43%. Tensile test measurements show a high yield strength on the cold rolled sample which decrease with annealing as expected. Fig. 7c also shows that the work hardening of the cold rolled sample exhibits at least three different stages of plastic deformation as the tensile test progresses. The first stage (I) corresponds to the slip of dislocations and deformation twins. On the second stage (II) the formation of martensite by deformation occurs and finally, on the third stage (III), all the deformation mechanisms interact until the failure of the tensile sample. This behavior was also observed by Ding et al. [13], but in this case, the authors divided the curve in four stages. In the present work, the authors do not take into account the elastic range, because it is not worth discussing uniform deformation if the material has not yielded or reach the elastic limit. In turn, an increase in deformation leads to saturation of the deformation twin formation. As found in literature, the austenitic grain of a 18Mn-0.06C steel is subdivided gradually as the deformation microtwins are formed [39], increasing the difficulty of nucleation and growth of new nuclei.

For the 18Mn-2.9Al-2.9Si and 0.04C steel Ding et al. [13] found an intense formation of $\varepsilon$-martensite on the third stage (III), finishing with the formation of $\alpha'$-martensite directly from the austenite, which at this stage is highly stressed, thereby facilitating the phase transformation. The formation of $\varepsilon$ martensite at 0.1 of true strain was also found by Liang et al. [40] on a 24Mn-0.01C steel and by Zhang et al. [41] on a 30Mn-4Si-2Al steel, both materials deformed at room temperature, however there was no $\alpha'$-martensite formation on both experiments.

## 5. Conclusions

- It was proved by transformation texture analysis that the reversion of austenite occurs without simultaneously recrystallization because the copper and brass components were strongly present on the samples.
- It was found that the formation of $\varepsilon$ martensite occurs during processing, and that it transforms immediately to $\alpha$ martensite, modifying significantly the mechanical behavior of the steel.
- The transformation induced by deformation occurs in two steps $\gamma \rightarrow \varepsilon \rightarrow \alpha'$ and $\alpha'$ martensite tends to be the major phase with the deformation increasing.
- Tensile test measurements show that there is a significant increase on the yield strength as the cold reduction

increases and that this difference remains after annealing of the samples, features which are extremely important for the application of this steel in the automotive industry.

## Conflict of interest

The authors declare no conflicts of interest.

## Acknowledgements

The authors would like to thank the FAPEMIG, CNPq and CAPES institutions for granting academic scholarships and financial support.

## REFERENCES

[1] Kim YG, Kim TW, Han JK, Chang RW. Development of new austenitic Fe-Mn-Al-C steels for automotive applications. Key Eng Mater 1993;84:461–72.
[2] Grässel O, Krüger L, Frommeyer G, Meyer LW. High strength Fe-Mn-(Al,Si) TRIP/TWIP steels development – properties – application. Int J Plast 2000;16:1391–409.
[3] Frommeyer G, Brüx U, Neumann P. Supra-ductile and high-strength manganese-TRIP/TWIP steels for high energy absorption purposes. ISIJ Int 2003;43:438–46.
[4] Dumay A, Chateau JP, Allain S, Migot S, Bouaziz O. Influence of addition elements on the stacking-fault energy and mechanical properties of an austenitic Fe-Mn-C steel. Mater Sci Eng A 2008;483:184–7.
[5] Bouaziz O, Allain S, Scott CP, Cugy P, Barbier D. High manganese austenitic twinning induced plasticity steels: a review of the microstructure properties relationships. Curr Opin Solid State Mater Sci 2011;15:141–68.
[6] Ray RK, Jonas JJ, Butrón-Guillén MP. Transformation texture in steels. ISIJ Int 1994;34:927–42.
[7] Rong-Gang X, Ren-Yu F, Qian L, Xi-Cheng W, Lin L. Tensile properties of TWIP steel at high strain rate. J Iron Steel Res Int 2009;16:81–6.
[8] De Cooman BC, Kwon O, Chin KG. State-of-the-knowledge on TWIP steel. J Mater Sci Technol 2012;28:513–27.
[9] Chen L, Zhao Y, Qin X. Some aspects of high manganese Twinning-Induced Plasticity (TWIP) steel. A review. Acta Metall Sin 2013;26:1–15.
[10] Santos DB, Salehn AA, Gazder AA, Carman A, Duarte DM, Ribeiro EAS, et al. Effect of annealing on the microstructure and mechanical properties of cold rolled Fe-24Mn-3Al-2Si-1Ni-0.06C TWIP steel. Mater Sci Eng A 2011;528:3545–55.
[11] Lu Y, Hutchinson B, Molodov DA, Gottstein G. Effect of deformation and annealing on the formation and reversion of e-martensite in an Fe-Mn-C alloy. Acta Mater 2010;58:3079–90.
[12] Lu Y, Molodov DA, Gottstein G. Recrystallization kinetics and microstructure evolution during annealing of a cold-rolled Fe–Mn–C alloy. Acta Mater 2011;59:3229–43.
[13] Ding H, Ding H, Song D, Tang Z, Yang P. Strain hardening behavior of a TRIP/TWIP steel with 18.8%Mn. Mater Sci Eng A 2011;528:868–73.
[14] Lu F, Yang P, Meng L, Cui F, Ding HJ. Influences of thermal martensites and grain orientations on strain-induced martensites in high manganese TRIP/TWIP steels. J Mater Sci Technol 2011;27:257–65.
[15] Sugimoto K, Usui N, Kobayashi M, Hashimoto S. Effects of volume fraction and stability of retained austenite on ductility of TRIP-aided dual-phase steels. ISIJ Int 1992;32:1311–8.
[16] Ofei KA, Zhao L, Sietsma J. Microstructural development and deformation mechanisms during cold rolling of a medium stacking fault energy TWIP steel. J Mater Sci Technol 2013;29:161–7.
[17] Fujita H, Katayama T. In-situ observation of strain-induced gamma-epsilon-alpha prime and gamma-alpha prime martensitic transformation in Fe-Cr-Ni alloys. Mater Trans JIM 1992;33:243–52.
[18] Bracke L, Verbeken K, Kestens L, Penning J. Microstructure and texture evolution during cold rolling and annealing of a high Mn TWIP steel. Acta Mater 2009;57:1512–24.
[19] Bracke L, Verbeken K, Kestens L. Texture generation and implications in TWIP steels. Scripta Mater 2012;66:1007–11.
[20] Bracke L, Kestens L, Penning J. Influence of $\alpha'$-martensite in an austenitic Fe-Mn-C-N alloy. Scripta Mater 2007;57:385–8.
[21] Liu JB, Liu XH, Liu W, Zeng YW, Shu KY. Microstructure and hardness evolution during isothermal process at 700°C for Fe-24Mn-0.7Si-1.0Al-TWIP steel. Mater Charact 2010;61:1356–8.
[22] Dafé SSF, Sicupira F, Matos F, Cruz N, Moreira D, Santos DB. Effect of cooling rate on ($\varepsilon$, $\alpha'$) martensite formation in twinning/transformation-induced plasticity Fe–17Mn–0.06C steel. Mater Res 2013;16:1229–36.
[23] Dafé SSF, Moreira D, Matoso MS, Gonzalez BM, Santos DB. Martensite formation and recrystallization behavior in 17Mn0.06C2Si3Al1Ni TRIP/TWIP steel after hot and cold rolling. Mater Sci Forum 2013;753:185–90.
[24] Jonas JJ. Transformations texture associated with steel processing. In: Suwas HS, Bhattacharjee D, editors. Microstructure and texture in steels. Springer; 2009. p. 3–16.
[25] Jonas JJ. Effect of austenite recrystallization on toughness of pipeline steels. Mater Sci Forum 2013;753:546–53.
[26] Ray RK, Jonas JJ. Transformation texture in steels. Int Mater Rev 1990;35:1–36.
[27] Somani MC, Juntunen P, Karjalainen LP, Misra RDK, Kyröläinen A. Enhanced mechanical properties through reversion in metastable austenitic stainless steels. Metall Mater Trans A 2009;40:729–44.
[28] Chapellier PH, Ray RK, Jonas JJ. Prediction of transformation textures in steels. Acta Metall Mater 1990;38:1475–90.
[29] Wang N, Huang JC. Texture analysis on hexagonal materials. Mater Chem Phys 2003;81:11–26.
[30] Liu Q, Ma Z, Gu N. The $\gamma \rightarrow \varepsilon$-martensitic transformation and its reversion in the FeMnSiCrNi shape-memory alloy. Metall Mater Trans A 1998;29:1579–83.
[31] Gauzzi F, Montanari R. Martensite reversion in an Fe–21%Mn–0.1%C alloy. Mater Sci Eng A 1999;273:524–7.
[32] Kowalska J, Ratuszek W, Witkowska M, Zielinska-Lipiec A. Development of microstructure and texture in Fe–26Mn–3Si–3Al alloy during cold-rolling and annealing. J Alloy Compd 2013, http://dx.doi.org/10.1016/j.jallcom.2013.12.059.
[33] Kumar MK, Samajdar I, Venkatramani N, Dey GK, Tewari R, Srivastava D, et al. Explaining absence of texture development in cold rolled two-phase Zr–2.5 wt% Nb alloy. Acta Mater 2003;51:625–40.
[34] Hiwarkar VD, Sahoo SK, Samajdar I, Narasimhan K, Mani Krishna KV, Dey GK, et al. Annealing of cold worked two-phase Zr-2.5 Nb-associated microstructural developments. J Nucl Mater 2009;384:30–7.
[35] Bunge HJ. Texture analysis in material science. Butterworth: London; 1982.
[36] Kocks UF, Tomé CN, Wenk HR, Mecking H. Texture and anisotropy preferred orientations in polycrystals and their effect on materials properties. Cambridge: Cambridge University Press; 1998.

[37] Johannsen DL, Kyrolainen A, Ferreira PJ. Influence of annealing treatment on the formation of nano/submicron grain size AISI 301 austenitic stainless steels. Metall Mater Trans A 2006;37:2325–38.
[38] Knutsson A, Hedström P, Odén M. Reverse martensitic transformation and resulting microstructure in a cold rolled metastable austenitic steel. Steel Res Int 2008;79:433–9.
[39] Jin JE, Lee YK. Strain hardening of a Fe-18Mn-0.6C-1.5Al TWIP steel. Mater Sci Eng A 2009;527:157–61.
[40] Liang X, McDermid JR, Bouaziz O, Wang X, Embury JD, Zurob HS. Microstructural evolution and strain hardening of Fe–24Mn and Fe–30Mn alloys during tensile deformation. Acta Mater 2009;57:3978–88.
[41] Zhang X, Sawaguchi T, Ogawa K, Yin F, Zhao X. Deformation microstructure of TRIP/TWIP Steels at the early deformation stages. ESOMAT 2009:1–8.